JSEE Vol. 26, No. 1, 2024 DOI: 10.48303/jsee.2024.2010550.1072

Research Paper

Numerical and Analytical Investigation of Reduced Beam Section with Yielding Damper and their Comparison

Kambiz Cheraghi[1*], Mehrzad TahamouliRoudsari[2], Sasan Kiasat[3] and Kaveh Cheraghi[4]

1. M.Sc. Student, Department of Civil Engineering, Faculty of Engineering, Razi University, Kermanshah, Iran, *Corresponding Author; email: kambiz.cheraghi@gmail.com
2. Associate Professor, Department of Civil Engineering, Kermanshah Branch, Islamic Azad University, Kermanshah, Iran
3. Ph.D. Student, Department of Civil and Environmental Engineering, AmirKabir University, Tehran, Iran
4. M.Sc. Student, Department of Mechanical Engineering, Engineering Faculty, Razi University, Kermanshah, Iran

Received: 31/05/2023
Revised: 13/12/2023
Accepted: 02/01/2024

ABSTRACT

Connections play a crucial role in structures, including steel structures, and have a significant impact on the seismic behavior of the structure. One particular type of connection commonly used in steel structures is the Reduced Beam Section (RBS). This connection reduces the moment strength of the beam near the column, which in turn results in less moment being transferred to the column at the final moment. The study involved 30 numerical analyses conducted using ABAQUS to examine two cases. The first case involved investigating a connection with a beam that had a hole in the flange area. The variables examined included the area of the flange holes and the axial force of the column. In the second case, a yield ring was utilized in the flange area of the beam. The radius of the yield ring was considered as a variable in six different cases. Equations for calculating the maximum strength moment and analyzing the linear region of a beam were presented in the study. The yielding damper must yield earlier than other members, and an equation was provided to ensure that it does. Finally, the cyclic behavior of the two models was also compared. Numerical analysis revealed that if the area of the flange holes is half that of the beam flanges, the beam's strength does not significantly decrease with increasing axial force. The elastic stiffness and ductility of the SRD-equipped connection were higher than the RBS model, with the SRD model achieving 1.8 and 2.6 times greater ductility and elastic stiffness, respectively, in the most optimal state.

Keywords:
Rigid connection; Yielding damper, Finite element analysis; Ring damper

1. Introduction

In moment-resisting frames, the structural connections must withstand moment and shear created under external loads (Mohamadi Tekantape et al., 2017; Mohammadi et al., 2020). If the external forces exceed a certain limit, they will cause damage in different parts of the structure, and by taking measures, these damages can be moved to parts of the structure so that the structure does not suffer premature instability. Among these arrangements in the rigid connections of steel structures is the weakening of the beam flanges near the connection area or RBS. In these connections, during an earthquake, plastic is formed in the weakened area of the connection, and a

large amount of energy from seismic loads is consumed, thus preventing stress concentration and brittle fractures in the welds and the metal surrounding the weld at the connection. However, from experimental studies, the lack of sufficient ductility capacity of rigid connections has been reported (Jin & El-Tawil, 2005; Momenzadeh et al., 2017; Ohsaki et al., 2009) optimized the reduced beam section of a cantilever H-beam under forced cyclic displacement. They used finite element analysis with Abaqus software, validating their results against experiments. Simulated annealing was employed to search for global optimal solutions. The optimization significantly improved energy dissipation capacity by optimizing the flange shape. Vajdian et al. (2020) studied the behavior of steel moment frames with different connections. The proposed connection with a replaceable drilled attachment part performed best, followed by a variable-diameter connection. The reduced flange connection ranked third. It resulted in minimal damage, making it a promising option for future designs. Miryahyavi et al. (2023) studied the cyclic behavior of sloped extended end-plate beam-to-column connections using the Finite Element Method. Results showed that increasing beam angle decreased ductility and moment-resisting capacity, but the models satisfied design code limitations. The study provides insights into the behavior of these connections under cyclic loading. Madjour et al. (2018) investigated the use of end plate connections to enhance the bending and shear capacity of cellular beams with web openings. Numerical simulations using Abaqus software were compared with experimental data from the literature. The study provides insights into the behavior of such beams with end plate connections. Tabar et al. (2022) investigated reduced web section (RWS) and reduced beam section (RBS) connections for retrofitting non-seismically designed buildings. Empirical fragility curves showed that RWS connections had significantly lower probabilities of exceeding certain inter-story drifts and collapse compared to RBS connections. Bompa et al. (2023) assessed the cyclic performance of reduced beam section (RBS) moment connections with larger member sizes than allowed by current seismic provisions. Results showed that connections with beam sections up to two times the limits exhibited a stable inelastic response. Still, very large beam sections showed significant hardening and increased susceptibility to weld fracture. The study suggests deeper RBS cuts and more stringent design requirements for connections with deep columns.

To improve the seismic behavior of structures, researchers have introduced different yielding elements; in the research conducted by Andalib et al. (2014) and Gorji Azandariani et al. (2020), steel ring dampers (SRD) were investigated numerically and experimentally. These researchers showed that these dampers behave better than pipe rings and show more ductility and energy dissipation.

Yield dampers are devices used in seismic-resistant structures to reduce the structural damage caused by earthquakes. They absorb energy by undergoing plastic deformation and reduce the forces acting on the structure (Cheraghi, Tavana, et al., 2023; Hosseini Hashemi & Keykhosrokiany, 2019; Sedaghatnezhad et al., 2021; TahamouliRoudsari et al., 2022; Zahrai & Heisami, 2017). Yield dampers work by yielding in a controlled manner and dissipating energy. They can be installed in new structures or used as a retrofit solution for existing ones (Tahamouli Roudsari et al., 2019). Yielding dampers in connections can reduce yielding in main members by concentrating the failure in the damper itself. For this purpose, researchers have been paying attention, and research has been done on the use of yielding damper in the connection. Bayat & Shekastehband (2019) proposed a new yielding damper called T-SSD to increase energy dissipation capacity and stiffness while reducing seismic damage in beam-to-column connections. Nonlinear finite element analysis showed satisfactory performances, with shear tab presence increasing initial stiffness by up to 25%. Latour et al. (2019) proposed a sliding hinge joint (SHJ) as a supplemental energy dissipation system for steel Moment Resisting Frames (MRFs). The SHJ system uses friction dampers to provide energy dissipation but lacks self-centering capacity due to high unloading stiffness. The study proposes a new layout that combines friction devices' threaded

bars with disk springs to introduce restoring forces and achieve self-centering capability. Experimental investigations and analysis of an MRF equipped with the proposed column base joints showed promising results. Ferrante Cavallaro et al. (2018) conducted an experimental investigation to study the cyclic behavior of three different friction shims used in Sliding Hinge Joints (SHJs) for seismic energy dissipation. The study focused on the dependence of friction coefficient on parameters such as bolt preloading, type of washers, and material variability. Results defined friction coefficient values for design and regression analyses and slip test data for simplified rigid-plastic modeling in seismic analyses. Lor et al. (2018) proposed a new beam-to-column connection using slit dampers to increase ductility and moment capacity in structures. The proposed connection was tested under cyclic loading and showed high seismic performance, rotational capacity, and moment capacity. Experimental observations showed no cracks or fractures in welds, and high energy absorption of the slit dampers prevented damage to other parts. Numerical models in Abaqus software agreed well with experimental results, indicating high energy dissipation and ductility in the proposed connection. Vajdian, Zahraei, et al. (2020) evaluated the impact of different steel connections on moment frames. Drilled connections with variable diameters, particularly the diamond-shaped hole model, showed the best performance and rotational stiffness compared to other connections. Ahmady Jazany (2018) studied the seismic performance of drilled flange (DF) connections, analyzing the impact of design parameters and proposing equations to estimate yield and plastic moment capacity. The study provides practical recommendations for DF connection seismic design. Shadman Heidari et al. (2020) discuss the use of reduced beam section connections to enhance seismic behavior and address drawbacks through novel drilled flange connections. Experimental and analytical studies validate improved performance.

The research began by verifying the numerical model with an experimental sample. The experimental model was a beam with holes in the flange that weakened the connection area. The performance of the connection is significantly affected by the diameter of the flange holes. To investigate the effect of increasing the radius of the flange holes and the axial force of the column, 18 non-linear static analyses were conducted. The radius of the holes was examined in three cases that had not been studied previously. To examine the effect of the axial load on the column, the critical load of the column was first calculated. Then, the column was subjected to this load in six different modes: 0, 0.1 F_u, ..., 0.5 F_u. In actual structures, a significant portion of the column's axial force remains constant throughout the structure's lifespan. However, depending on the floor, the magnitude of this force varies. The study also took into account the impact of this force on the connection, which was close to the actual situation.

In the second case, numerical analyses were performed on a beam equipped with an SRD, which had not yet been investigated to improve the seismic behavior of a rigid connection. One of the important considerations in designing the yielding damper in the connection is that it must yield earlier than the beam and column. An equation was presented to ensure the damper would yield earlier than the beam. For analyzing this beam at the damper connection, equations were presented according to which the stress in the beam and SRD can be calculated in the linear and non-linear regions. Additionally, parametric studies were conducted to investigate the effect of the SRD on the connection. The purpose of the RBS beam is to reduce the transmission moment to the column during an earthquake. When equipped with a damper, the transfer moment can be adjusted by changing the dimensions of the damper. For this reason, this research compares and analyzes both options.

It is important to note that there haven't been any numerical studies conducted on the effect of the area of the flange holes of the beam, along with the axial force of the column on it. This research aims to partially solve the ambiguities in this field. Although many yield dampers have been proposed for connections (Banisheikholeslami et al., 2016; Ferrante Cavallaro et al., 2018; Molavi et al., 2020), this study proposes the use of a ring

damper designed for steel structure connections, which so far hasn't been numerically investigated. This proposal can help resolve uncertainties in this field.

2. Parametric Study of RBS

2.1. Numerical Model Validation

In this section, the effect of the flange hole on the connection performance is investigated; for this purpose, the experimental research of TahamouliRoudsari et al. (2018) was used to validate the numerical model. In this experimental model, an RBS connection (without column) has been investigated according to Figure (1a), which has four holes on its flange. The loading in this research was cyclical at the free end of the beam, whose moment-drift ratio diagram is shown in Figure (1b).

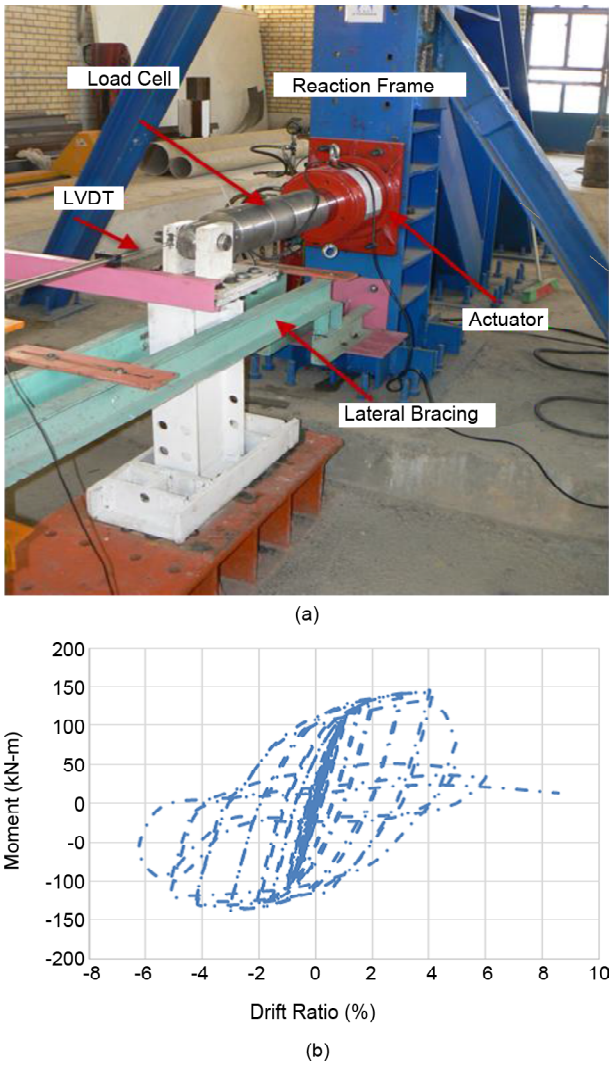

Figure 1. (a) Experimental setup and (b) Hysteresis diagram result (TahamouliRoudsari et al., 2018).

An 8-node solid element was used to model the numerical model. Each of these nodes has three translation degrees of freedom, including 24 degrees of freedom. The meshing of the model was done using 0.5 cm elements, which is shown in Figure (2a). The analysis was done in Abaqus using the implicit solver in quasi-static mode, and the load was applied monotonic to the end of the beam. In the numerical model, the influence of the non-linear behavior of materials and large deformations was also considered. The analysis of the models was done by the control displacement method. Newton-Raphson methods were also used to analyze finite element models (Aghani et al., 2023; Cheraghi, TahamouliRoudsari, & Kiasat, 2023). After the analysis, its results were compared with the experimental model, which is shown in Figure (2b). It can be seen that the results were close to each other with good accuracy so that it can be used for other analyses.

Figure (3a) and 3b show the conditions of the numerical model and the experimental after loading, respectively. It can be observed that the numerical model can predict the failure behavior of the experimental sample to an acceptable extent.

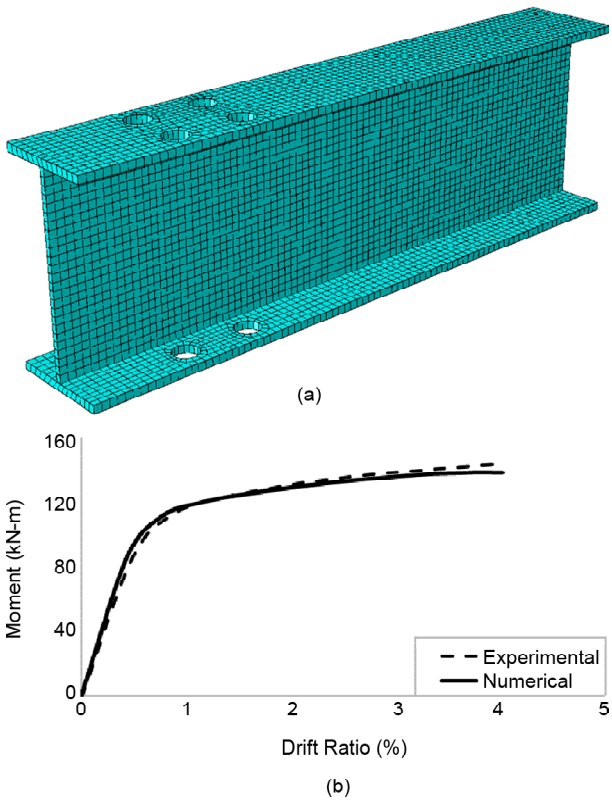

Figure 2. (a) FEM model and (b) Comparison of moment-drift curves between experimental and numerical results.

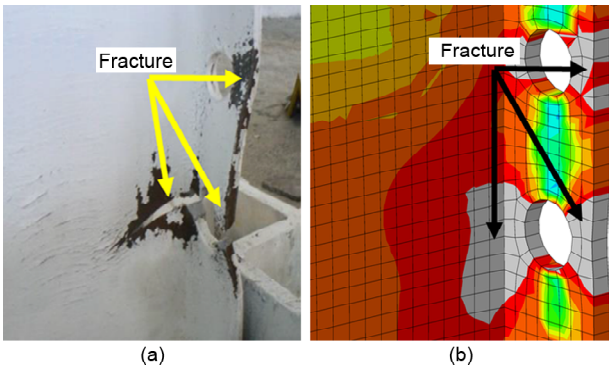

Figure 3. Failure area in the (a) numerical and (b) experimental model after loading (TahamouliRoudsari et al., 2018).

2.2. Introduction of Parametric Models

In this section, the RBS beam was modeled and analyzed in the state connected to the column to consider a more realistic state of the model. The investigated model is an external connection of the structure, whose boundary conditions, dimensions, and forces applied to it are shown in Figure (4). More details of this model, including the sections used and the location of the holes, are presented in Figures (5a) and (5b). The stress and strain characteristics of the steel in the numerical model are shown in Figure (5c).

The model comprises two variables: the ratio of the area of the flange holes to the total area (Equation 1) and the axial force of the column.

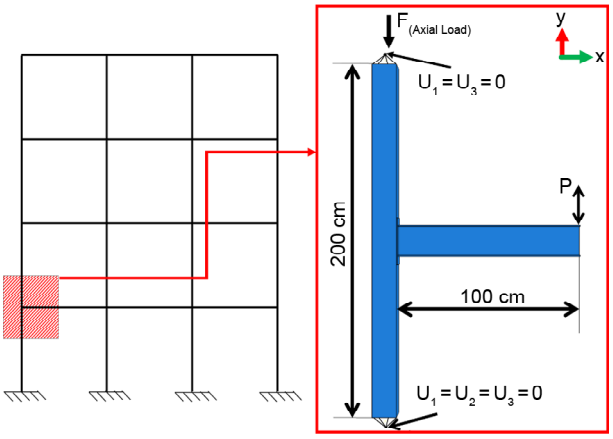

Figure 4. Boundary conditions of the numerical model.

The area of the hole in 3 cases was introduced according to the second column of Table (1). The axial force of the column in six cases is expressed as a percentage of the column's critical load, which is introduced in the third column of Table (1). Here, F_u denotes the axial force of the column, calculated as 2010.6 KN according to the American Steel Code ANSI/AISC 360-16 (Committee, 2010). The numerical model's analysis in this section was performed in two steps: the axial force of the column and displacement of the beam end were applied in the first and second steps, respectively. Table (1) shows that the models are named based

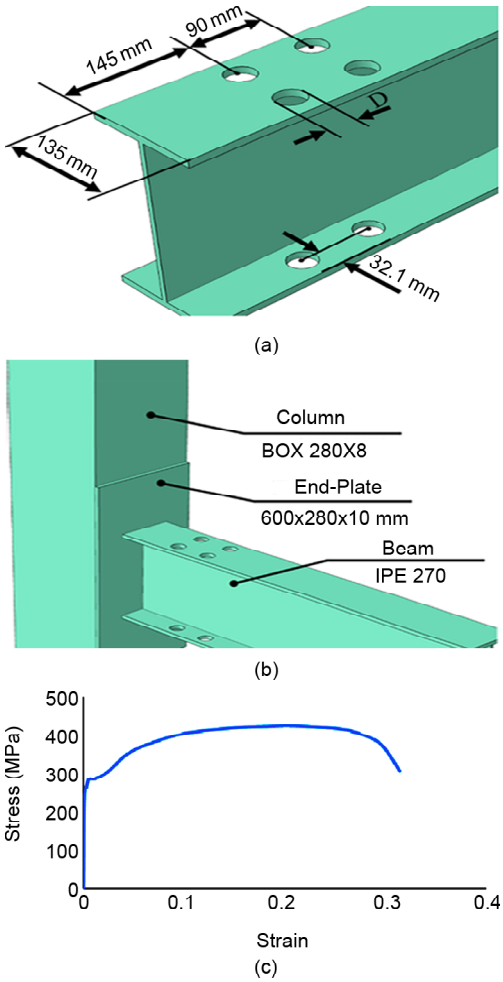

Figure 5. (a) The details of the holes in the model, (b) The sections used in the model, and (c) The strain stress diagram of the used steel.

Table 1. Specifications of numerical models.

Name	α (%)	Column Axial Load (F)
M1-25-0, M-125-0.1, …, M1-25-0.5	25	0, 0.1 F_u, …, 0.5 F_u
M1-50-0, M1-15-0.1, …, M1-50-0.5	50	0, 0.1 F_u, …, 0.5 F_u
M1-75-0, M1-75-0.1, …, M1-75-0.5	75	0, 0.1 F_u, …, 0.5 F_u

on the connection type, α, and the axial force of the column. Specifically, the M1-25-0.1 model represents the RBS connection model, where "α" equals 25%, and the axial force of the column is 10% of its critical load.

$$\alpha = \frac{2D_{mm}}{135} \quad (1)$$

After conducting the numerical analysis, the moment-drift diagrams of the models were extracted, as shown in Figure (6). It is evident that in all models, there was no drop until the end of loading as long as the axial force was equal to 0.1 F_u and 0.2 F_u. The model with an axial force of 0.3 F_u experienced premature failure only when the value of α was equal to 25. In all models, when the axial force of the column was equal to 0.5 F_u, the graphs of the models with α equal to 25, 50, and 75 experienced a drop in drift of 2.8, 2.6, and 3.17, respectively.

Figure (7a) shows the maximum moment of the models. In this diagram, the horizontal axis shows the ratio of the axial force of the column to its critical force, as can be seen. The addition of axial load has reduced the results in all cases. Also, in the case that the axial force of the column is 0.5 times the critical load, the maximum moment is independent of the "α". Figure (7b) shows the maximum moment drift in the model. Or the moment of zero stiffness of the model can be considered. The models with "α" equal to 0.25 and 0.5 have very similar results, while a sharp decrease is observed in the model with α = 0.75.

Also, to calculate the ductility and elastic stiffness of the models, the equivalent bilinear diagram was calculated according to the FEMA (Council, 2006) Figure (8).

Then, according to Equations (2) and (3), elastic stiffness and ductility were calculated. Figure (9) shows some examples of the results and its equivalent bilinear diagram.

$$K_e = M_y / D_y \quad (2)$$

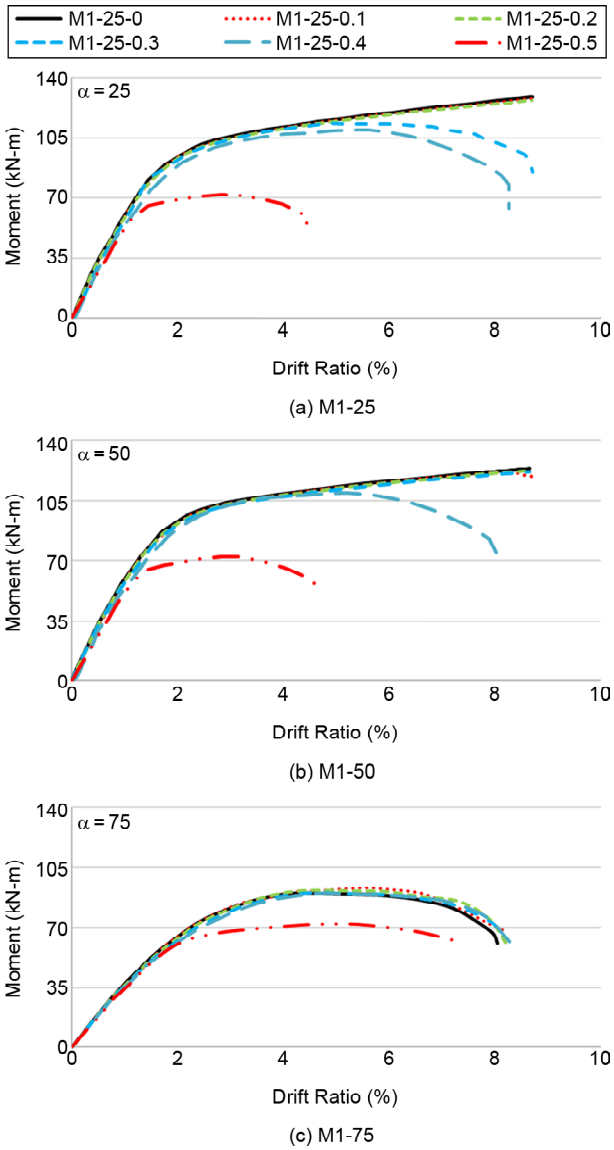

Figure 6. Results of numerical models.

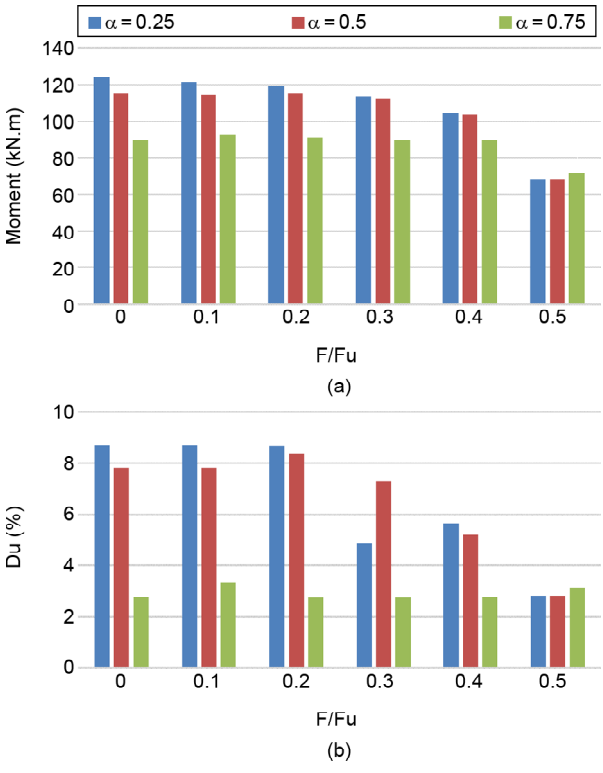

Figure 7. Results of (a) Maximum moment and (b) drift as maximum moment.

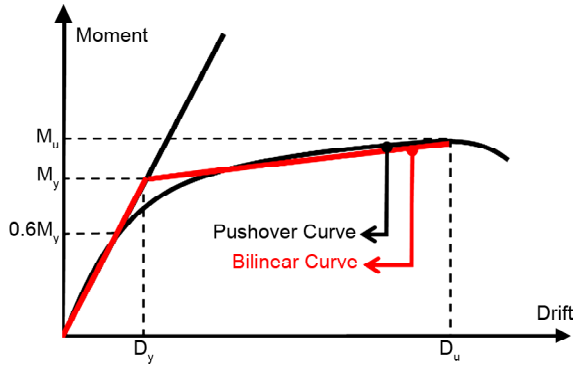

Figure 8. The backbone curve and equivalent bilinear.

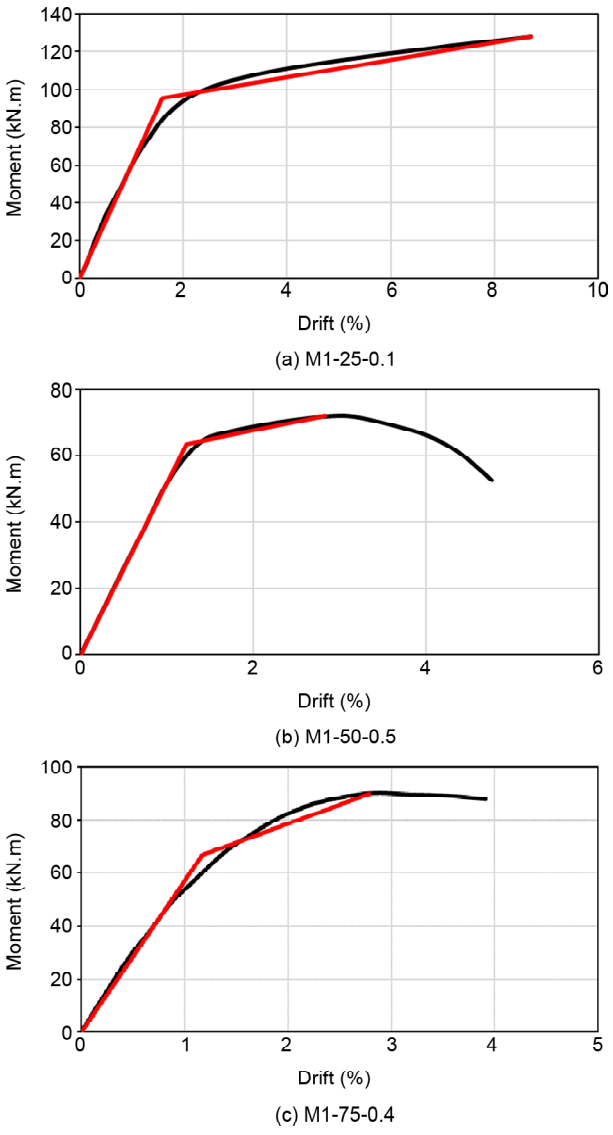

Figure 9. The non-linear and bi-linear curves are equivalent to models.

$$Ductility = D_u / D_y \quad (3)$$

Figure (10a) shows the ductility results of the samples. As can be seen, in the model with "α" equal to 0.75, increasing the axial force does not affect the results. In models with "α" equal to 0.25 and 0.5, the addition of axial force has reduced the ductility. The ductility of models with α = 0.75 has decreased significantly compared to other results. Also, the results of elastic stiffness are shown in Figure (10b). It can be seen that the elastic stiffness decreased almost linearly with the increase of the axial force. Also, the results of the elastic stiffness of models with α = 0.25 and α = 0. 5 are almost the same.The contour of three examples of the models is shown in Figure (11).

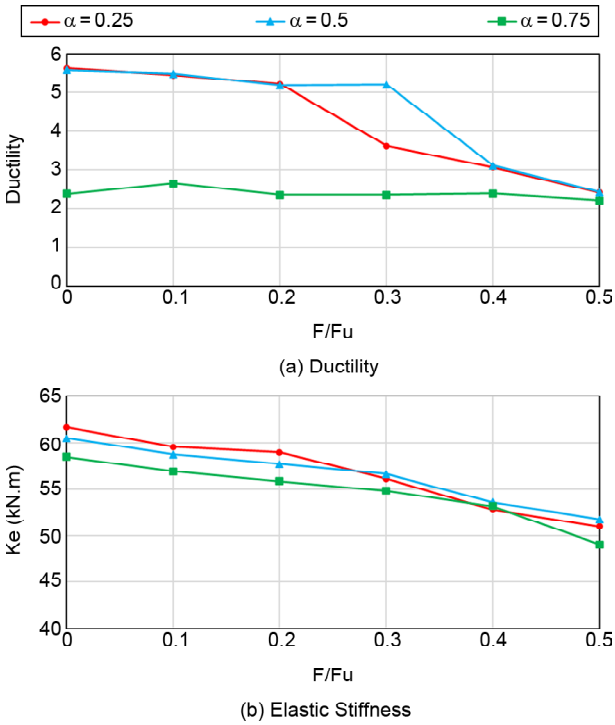

Figure 10. The results of a) Ductility and b) Elastic stiffness.

3. Effect of Yielding Damper on Connection

The experimental sample of Andalib et al. (2014) was used to validate the steel rings model. Figure (12a) shows the dimensions and details of the experimental model, and Figure (12b) shows the displacement force diagram result of this model.

To calculate the moment diagram in SRD using symmetry, its mathematical model is according to Figure (13a). The diagram of the internal moment of the ring is shown in Figure (13b). The internal moment equation in this part of SRD is in the form of Equation (4). It can be seen that the maximum moment occurred in SRD at the point of force application. Additionally, the moment in the ring

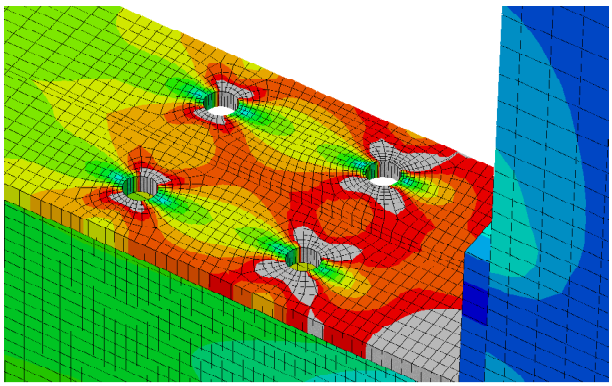

(a) M1-25

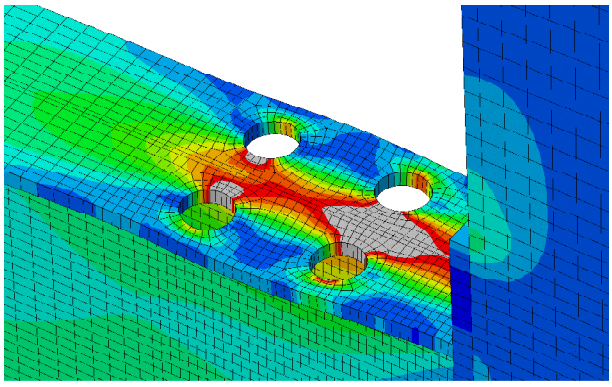

(b) M1-50

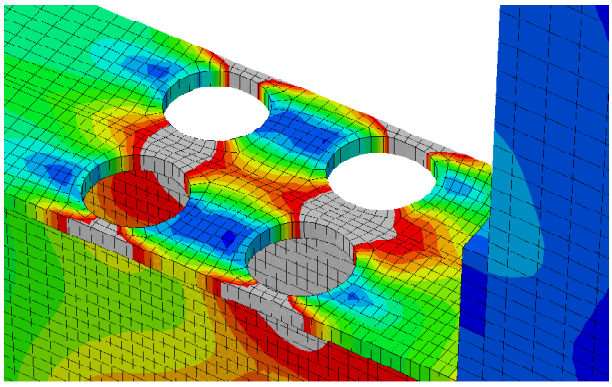

(c) M1-75

Figure 11. Stress contour at the moment of beam yielding for models.

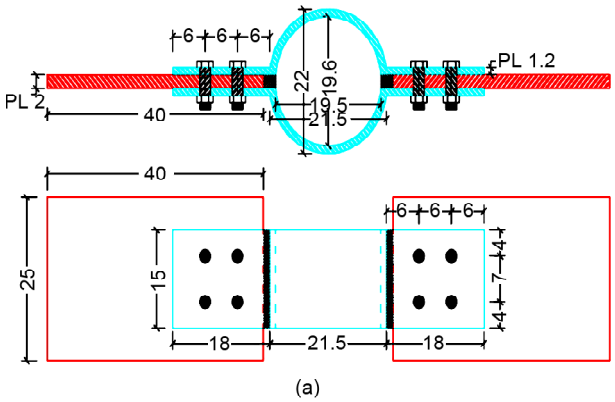

(a)

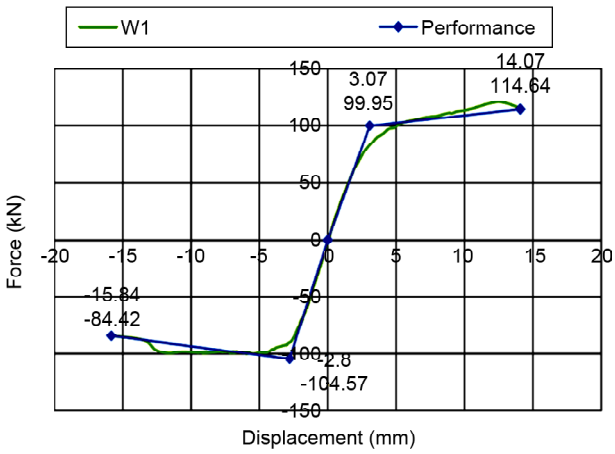

(b)

Figure 12. (a) The dimensions of the experimental sample for verification and (b) The results of its force-displacement diagram (Andalib et al., 2014).

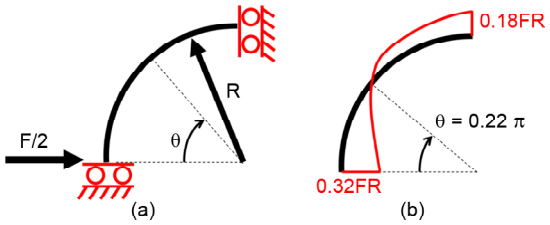

Figure 13. (a) Mathematical model of SRD and (b) Internal moment diagram of SRD.

was equal to zero at an angle of 0.22π Rad. The yield force (Roark et al., 1976) and elastic stiffness (Gorji Azandariani et al., 2020) of SRD are reported according to Equations (5) and (6), respectively. The yield stress of SRD is reported to be 345 MPa.

$$M(\theta) = 0.32FR - 0.5FR\sin(\theta) \quad (4)$$

$$F_y = \frac{t_s^2 L}{R}\sigma_{y_s} \quad (5)$$

$$k_s = 945000L\left(\frac{t_s}{2R}\right)^3 (N/mm) \quad (6)$$

A shell element was used to numerically model the yield ring because the ratio of its dimensions to its thickness was greater than 10 (Abaqus, 2014). In the experimental model, it was reported that all failures occurred in the ring area, and no yielding occurred in the bolts or connection area. Therefore, the bolts were not included in the numerical model. Figure (14a) displays the stress contour of the numerical model at the end of loading, which indicates failure at the final moment of 4 points of the yielding ring. Additionally, stress was minimal at points where the moment was zero (Figure 13b). Figure (14b)

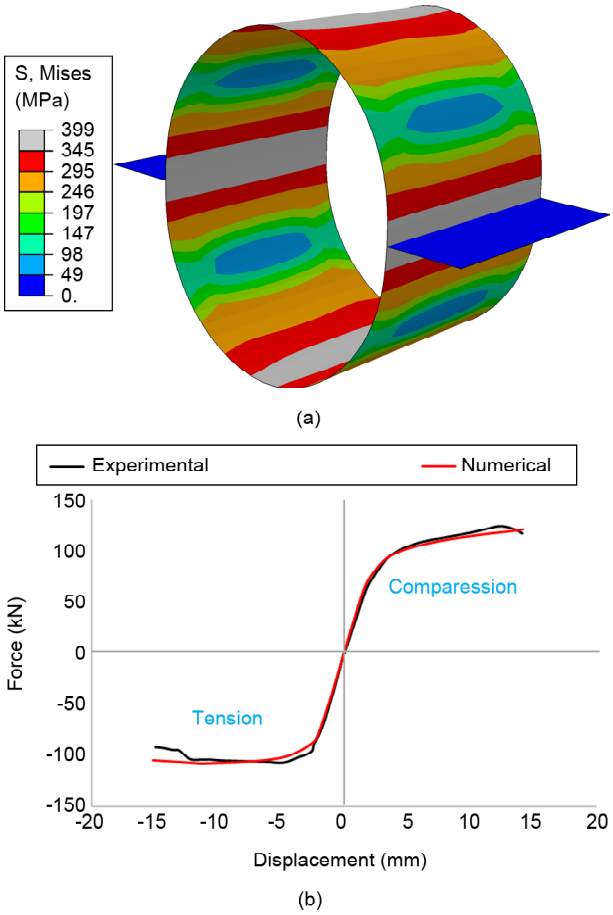

Figure 14. (a) Stress contour at the end of loading and (b) Comparison of numerical and experimental model results.

compares the numerical model results and the experimental in tension and pressure. It shows that the results of the numerical model and the experimental are reasonably close to each other.

3.1. Parametric Investigation of the Effect of SRD on the Beam

This section examines a beam with the same dimensions as the one in Section 2, but instead of flange holes, an SRD was added to the beam, as shown in Figure (15). All specifications and dimensions used in this model are similar to those of the RBS and SRD models. The SRD was connected to the beam using the Tie constraint in the numerical model. The variables in this case are the SRD radius, which is introduced in six modes: 20, 30, 40, 50, 60 and 70 mm. The models are named in a way that represents their SRD radius; for example, M2-20 represents a model with an SRD radius of 20 mm.

The key to using a yielding damper lies in its early yielding compared to other structural elements.

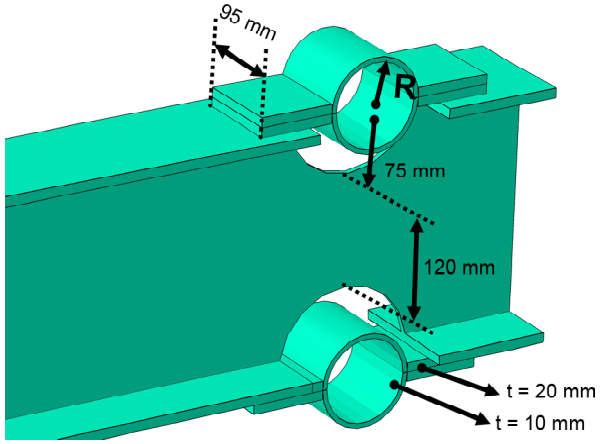

Figure 15. Dimensions and specifications of the M2 model.

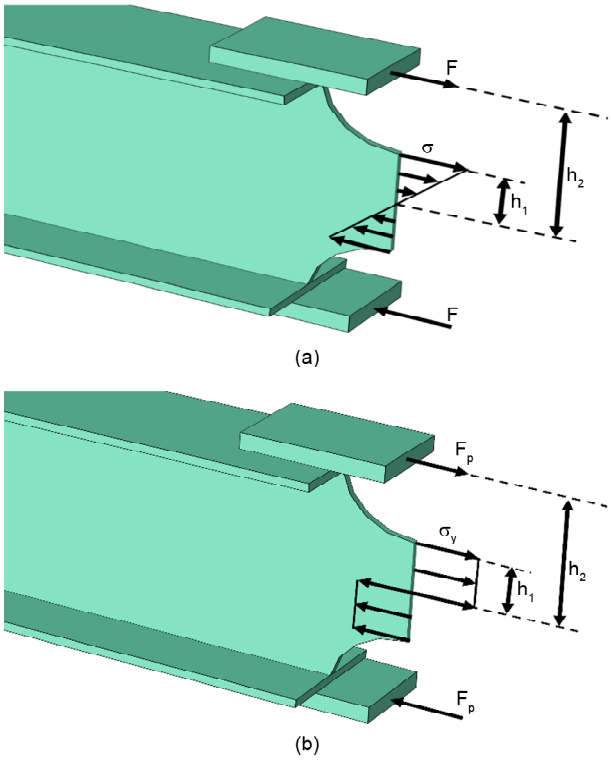

Figure 16. The behavior of the model in the state of (a) elastic and b) plastic.

To achieve early yielding of the damper, the beam moment contribution (Equation 7) and SRD should be calculated first, and then the dimensions should be adjusted to ensure yielding occurs first in the SRD and then in the beam. An equation in the form of Equation (8) was presented for the purpose of ensuring that yielding occurs first in the SRD region.

Figure (16a) displays stress in the linear range, while Figure (16b) shows the yield at the ultimate moment. The ultimate moment can be calculated using Equation (10).

$$M_b = \frac{E\, t_w h_1^3}{E\, t_w h_1^3 + 3dK_s h_2^2} M \quad (7)$$

$$\frac{\sigma_{y_b}}{\sigma_{y_s}} > 1.424 \frac{R^2}{t_s d}\left(\frac{h_1}{h_2}\right) = \propto \quad (8)$$

$$M_p = M_{pb} + M_{pr} \quad (9)$$

$$M_p = t_w h_1^2 \sigma_{y_b} + 2\frac{t_s^2 L}{R} h_2\, \sigma_{y_s} \quad (10)$$

Figures (13a) and (13b) show the moment of the first yielding in models M2-40 and M2-60, respectively. In the M2-40 model, initial yielding occurred in the ring damper, while in the M2-60, it took place in the beam region. According to Equation (8), the $\propto$ coefficient values for the M2-40 and M2-60 models are 0.47 and 1.06, respectively. Based on Equation (8), if the yield stress of two members (beam and SRD) are equal, yielding occurs first in the SRD if $\propto < 1$, and the opposite occurs if $\propto > 1$. This result is deduced by the numerical model, according to Figure (17).

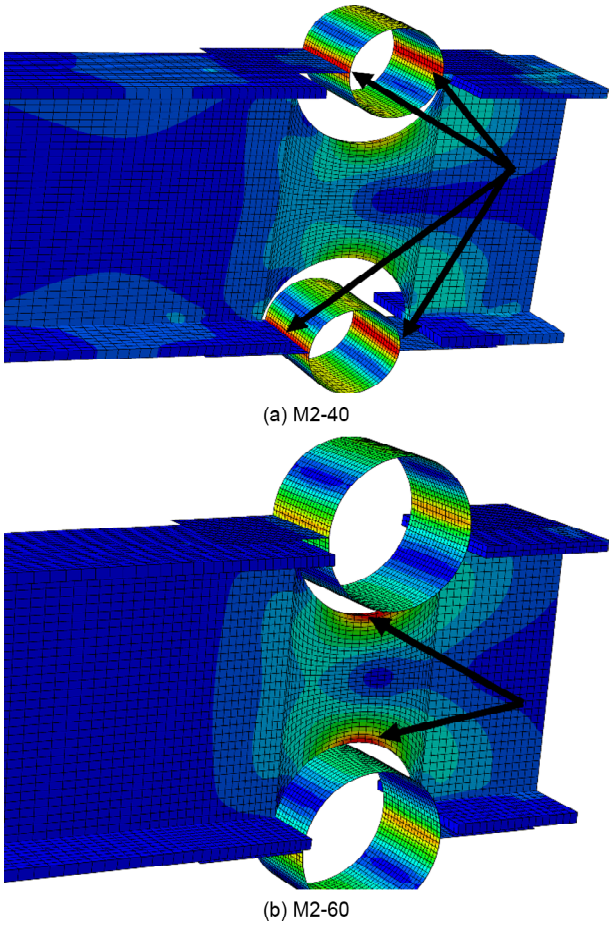

(a) M2-40

(b) M2-60

Figure 17. The areas of maximum stress in the models.

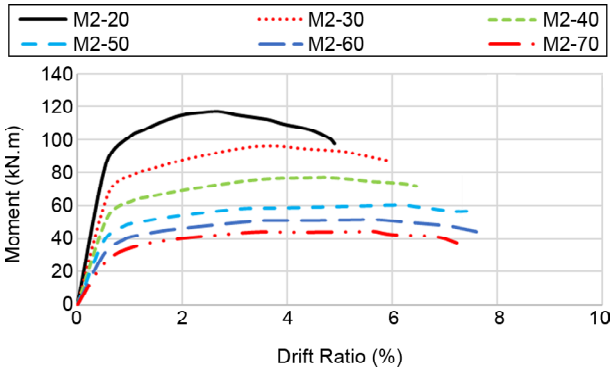

Figure 18. Numerical results of moment-drift diagram for beam (without column) equipped with SRD.

Figure (18) shows the moment-drift diagram of the beam equipped with SRD. It is obvious that the stiffness and maximum moment of the connection increased with the decrease in SRD radius. In models with a small yield ring radius ($\propto << 1$), a large part of the moment is transferred to the SRD. In the same way, early yield causes the curve of results to drop earlier. After yielding, all the moment is transferred to the beam web, causing rapid hinge formation in the beam. Increasing the radius of the yield SRD increased the ductility of the connection, resulting in M2-50 and M2-60 models having the latest moment of drop in the diagram. The coefficients α (Equation 8) for both models are close to 1, indicating that yielding begins simultaneously in the SRD and beam. One of the primary benefits of using a beam equipped with SRD is the ability to adjust its ultimate moment. According to Figure (18), the moment of the beam can be modified to any desired value.

After obtaining the bilinear diagrams results of Figure (18), the elastic stiffness and ductility were calculated and presented in Figure (19). Figure (19a) displays the M2 model ductility results. This graph's right vertical axis shows normalized results relative to the maximum ductility of M1 models (Figure 10a), which is 5.5. The graph indicates that as the damper's radius increases up to 50 cm, ductility increases and then decreases. Additionally, most models show higher ductility than the M1 model. In the best case, the model's ductility is 1.8 times that of the M1 model.

The graph presented in Figure (19b) displays the elastic stiffness outcomes in relation to the

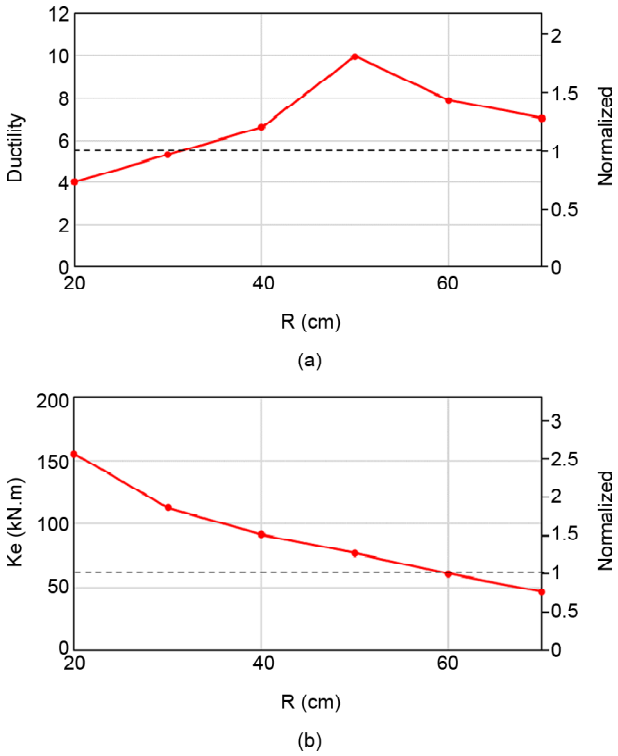

Figure 19. The results of (a) ductility and (b) elastic stiffness of M2 models.

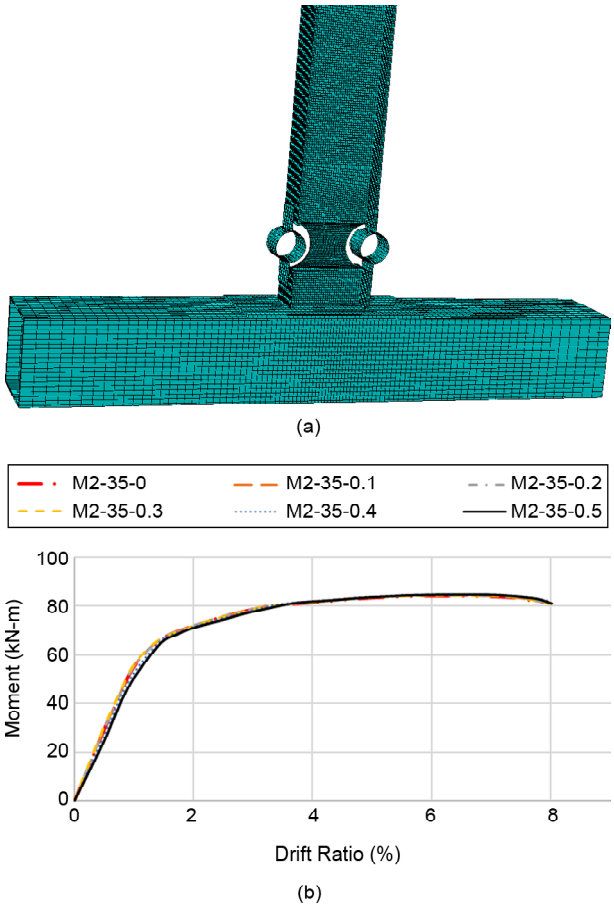

Figure 20. (a) Numerical model and (b) The effect of the axial force of the column on the moment-drift diagram.

radius of the damper. It is evident from the graph that an increase in the damper radius results in a decrease in the elastic stiffness. The vertical axis on the right side of the graph illustrates normalized outcomes in comparison to the maximum elastic stiffness of the M1 models from Figure (10b), which was 61 kN.mm. Also, in the best case, the elastic stiffness is 2.6 times the maximum elastic stiffness of M1 models.

3.2. Parametric Study of Connection with Columns for Beam Equipped with SRD

As previously mentioned, one of the benefits of using a beam equipped with SRD is the ability to adjust its ultimate moment by manipulating the SRD parameters. In this section, the beam model equipped with SRD and a column was examined (as shown in Figure 20a). Through a process of trial and error, the radius of the SRD was adjusted to minimize any damage to the column at the final moment. After doing this, the M2-35 model behaved better than the rest of the models; for this purpose, it was examined under different axial forces, the results of which are shown in Figure (19b). In Figure (20b), the M2-35-0.3 model is represented by an SRD radius of 35 mm and a load on the column equal to 0.3 times the critical load. It is evident that the axial force did not diminish the strength nor cause a premature drop of the diagram in any of the modes.

4. Comparison of the Cyclic behavior of the Models

For a more accurate comparison between the models, their cyclic behavior was examined in this section. Specifically, the M1-0.25 and M2-35 models were selected due to their better performance compared to the other models and were compared here. All model specifications remained unchanged from previous analyses, with the exception of loading, which was based on Table (2). As can be seen, the connection drift up to 0.04 is considered according to the experimental example.

After conducting an analysis, the hysteresis diagram of the two models was calculated as shown in Figure (12a). The seismic behavior of a connection is characterized by its dissipation of energy under cyclic loading (Cheraghi et al., 2023).

Table 2. Loading protocol and cycles(Roudsari et al., 2018).

Number of Cycles	Drift (rad)
6	0.00375
6	0.005
6	0.0075
4	0.01
2	0.015
2	0.02
2	0.03
2	0.04

This energy dissipation is determined by calculating the area enclosed by the moment-drift curve in each cycle. To provide a better comparison of the results, the cumulative energy dissipation diagram of the models was calculated in Figure (12b) relative to the drift ratio. It can be observed that the M1-0.25 model dissipates more energy than the M2-35 model. Additionally, at a drift ratio of 0.04, the energy dissipation of both models becomes closer to each other. At this point, the energy dissipation of the M1-0.25 model was found to be 8% more than the M2-35 model.

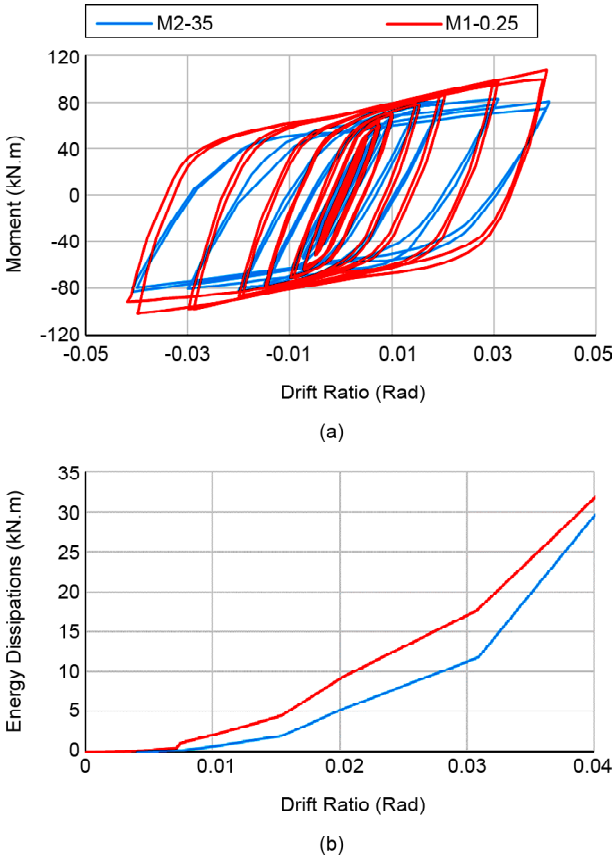

Figure 21. (a) The hysteresis diagram of the results of M1-0.25 and M2-35 models and (b) cumulative energy dissipation results.

5. Conclusion

In the second case, a ring yielding damper was added to the beam flanges and investigated. At first, an analytical equation was presented to calculate the stress in the linear and non-linear region of the beam model with yielding damper. The results of the models included maximum strength, ultimate drift, ductility, and elastic stiffness of the model. In the second case, a ring-yielding damper was added to the flanges of the beam and investigated. Initially, an analytical equation was presented to calculate the stress in the linear and non-linear regions of the model. For further investigations, the numerical model was analyzed in six cases where the radius of the column-free yield rings was varied. Finally, the beam model with SRD, which had the best answer in the previous step, was modeled along with the column, and its results were compared with the beam model with holes. To compare the energy loss of the models, cyclic analysis was performed on the models with better behavior in the previous step. The results of this research can be summarized as follows:

- If the axial force of the column is less than 0.3 F_u, the performance of the models with the ratio of the area of the holes to the total flange equal to 25% or 50% was almost the same.
- The RBS connection works best when the whole area to flange area ratio is 50%. In this case, it is guaranteed that the connection will not lose its strength due to the increase of the axial force of the column up to 0.4 F_u.
- The ductility of the models with α = 0.75 was independent of the column axis force. Also, increasing the area of the holes and the axial force of the column reduced the elastic stiffness of the RBS model.
- The presented equations allow the analysis of the beam with SRD in the linear region. An equation was presented according to which the model can be designed so that the onset of yielding is from the yielding damper. Also, the numerical model confirmed the correctness of the results of this equation.
- When the coefficient $\propto$ (Equation 8) is close to 1, the beam model with a yielding ring has

better ductility behavior than other models.
- If the stiffness of the SRD is too high ($\propto$ <<1), the stiffness and strength of the connection increase, but the ductility decreases.
- As the yield ring radius increased up to 50 cm, the ductility increased and then decreased. Also, increasing the radius of the damper decreased the elastic stiffness of the model. The ductility and elastic stiffness of the models with yielding damper were higher than RBD. So in the best case, the elastic stiffness and ductility of the connection equipped with a damper was 2.6 and 1.8 times that of the RBS connection. Comparing the total energy dissipation of the models also showed that the total energy dissipation of the M1-0.25 model was 8% more than the M2-35 model.
- By adding a yielding damper to the beam, the transfer moment to the column can be adjusted such that minimal damage is caused to the column at the final moment.
- The results of the numerical analysis of the beam with damper showed that if the SRD is designed correctly, even with the increase of the axial force of the column up to 0.5 F_u, there is no resistance reduction in the connection until the end of loading.

References

Abaqus, G. (2014). *Dassault Systemes Simulia Corporation*. Providence, Rhode Island, USA.

Aghani, H., Cheraghi, K., & Bakhshipour, M. (2023). *Numerical Investigation of the Effect of Aluminum Yielding Damper for the Retrofitting of Semi-rigid Steel Frames*. Periodica Polytechnica Civil Engineering. https://doi.org/https://doi.org/10.3311/PPci.23119.

Ahmady Jazany, R. (2018). Improved design of drilled flange (DF) moment resisting connection for seismic regions. *Bulletin of Earthquake Engineering*, *16*(5), 1987-2020. https://doi.org/https://doi.org/10.1007/s10518-017-0265-9.

Andalib, Z., Kafi, M. A., Kheyroddin, A., & Bazzaz, M. (2014). Experimental investigation of the ductility and performance of steel rings constructed from plates. *Journal of Constructional Steel Research*, *103*, 77-88. https://doi.org/https://doi.org/10.1016/j.jcsr.2014.07.016.

Banisheikholeslami, A., Behnamfar, F., & Ghandil, M. (2016). A beam-to-column connection with visco-elastic and hysteretic dampers for seismic damage control. *Journal of Constructional Steel Research*, *117*, 185-195. https://doi.org/https://doi.org/10.1016/j.jcsr.2015.10.016.

Bayat, K., & Shekastehband, B. (2019). Seismic performance of beam to column connections with T-shaped slit dampers. *Thin-Walled Structures*, *141*, 28-46. https://doi.org/https://doi.org/10.1016/j.tws.2019.04.010.

Bompa, D.V., Elghazouli, A.Y., Bogdan, T., Eatherthon, M.R., & Leon, R.T. (2023). Inelastic cyclic response of RBS connections with jumbo sections. *Engineering Structures*, *281*, 115758. https://doi.org/https://doi.org/10.1016/j.engstruct.2023.115758.

Cheraghi, K., TahamouliRoudsari, M., & Kiasat, S. (2023). Numerical and analytical investigation of U-shape dampers and its effect on steel frames. *Structures*, *55*, 498-509. https://doi.org/https://doi.org/10.1016/j.istruc.2023.06.037.

Cheraghi, K., TahamouliRoudsari, M., Kiasat, S., & Esfandiari, J. (2023). *Numerical Investigation of Cyclic Behavior of Angled U-shaped Yielding Damper on Steel Frames*. Periodica Polytechnica Civil Engineering. https://doi.org/10.3311/PPci.23213.

Cheraghi, K., Tavana, M. H., & Aghayari, R. (2023). *Investigating the Effect of Low-Yield Yielding Dampers on the Seismic Behavior of Steel Frames*. Periodica Polytechnica Civil Engineering. https://doi.org/https://doi.org/10.3311/PPci.21804.

Committee, A. (2010). *Specification for Structural Steel Buildings (ANSI/AISC 360-10)*. American Institute of Steel Construction, Chicago-Illinois.

Council, B.S.S. (2006). *NEHRP Recommended Provisions: Design Examples (FEMA 451)*. Federal Emergency Management Agency, Washington, DC, 05-05.

Ferrante Cavallaro, G., Francavilla, A. B., Latour, M.,

Piluso, V., & Rizzano, G. (2018). Cyclic response of low yielding connections using different friction materials. *Soil Dynamics and Earthquake Engineering*, *114*, 404-423. https://doi.org/https://doi.org/10.1016/j.soildyn.2018.07.041.

Gorji Azandariani, M., Abdolmaleki, H., & Gorji Azandariani, A. (2020). Numerical and analytical investigation of cyclic behavior of steel ring dampers (SRDs). *Thin-Walled Structures*, *151*, 106751. https://doi.org/https://doi.org/10.1016/j.tws.2020.106751.

Hosseini Hashemi, B., & Keykhosrokiany, B. (2019). Buckling response and elastic stiffness of butterfly dampers. *Journal of Seismology and Earthquake Engineering*, *21*(4), 11-20. https://doi.org/10.48303/jsee.2019.243312.

Jin, J., & El-Tawil, S. (2005). Seismic performance of steel frames with reduced beam section connections. *Journal of Constructional Steel Research*, *61*(4), 453-471. https://doi.org/https://doi.org/10.1016/j.jcsr.2004.10.006.

Latour, M., Rizzano, G., Santiago, A., & Simoes da Silva, L. (2019). Experimental response of a low-yielding, self-centering, rocking column base joint with friction dampers. *Soil Dynamics and Earthquake Engineering*, 116, 580-592. https://doi.org/https://doi.org/10.1016/j.soildyn.2018.10.011.

Lor, H. A., Izadinia, M., & Memarzadeh, P. (2018). Experimental and numerical study of I-shape slit dampers in connections. *Latin American Journal of Solids and Structures*, *15*(11). https://doi.org/https://doi.org/10.1590/1679-78254416.

Madjour, A., Soltani, M.R., & Harkati, E.H. (2018). A numerical investigation into the ultimate strength of steel cellular beams with semi-rigid connections. *Periodica Polytechnica Civil Engineering*, *62*(2), 517-532. https://doi.org/https://doi.org/10.3311/PPci.11304.

Miryahyavi, M., Khani, R., & Hosseinzadeh, Y. (2023). Evaluating the cyclic behavior of the sloped extended end-plate beam-to-column connections. *Periodica Polytechnica Civil Engineering*, *67*(2), 552-560. https://doi.org/https://doi.org/10.3311/PPci.21260.

Mohamadi Tekantape, J., Nouri, G.R., Ghanbari, A., & Erfani, A. (2017). Fragility curves for vulnerability assessment of steel moment-resisting frames adjacent to slopes. *Journal of Seismology and Earthquake Engineering*, 19(1), 37-47. http://www.jsee.ir/article_240754_e393435ac1309e753e0b18e4ba76f4d6.pdf.

Mohammadi, M., Nasirzadeh, N., & Kordbagh, B. (2020). Influence of debris impact on progressive collapse of a steel structure building. *Journal of Seismology and Earthquake Engineering*, *22*(3), 59-71. https://doi.org/10.48303/jsee.2020.248311.

Molavi, R., Izadinia, M., & Shahidi, A.R. (2020). Numerical and experimental studies on cyclic behavior of beam-to-column connection with yielding steel damper. *International Journal of Steel Structures*, *20*(2), 480-492. https://doi.org/https://doi.org/10.1007/s13296-019-00298-0.

Momenzadeh, S., Kazemi, M.T., & Asl, M.H. (2017). Seismic performance of reduced web section moment connections. *International Journal of Steel Structures*, *17*(2), 413-425. https://doi.org/https://doi.org/10.1007/s13296-017-6004-x.

Ohsaki, M., Tagawa, H., & Pan, P. (2009). Shape optimization of reduced beam section under cyclic loads. *Journal of Constructional Steel Research*, *65*(7), 1511-1519. https://doi.org/https://doi.org/10.1016/j.jcsr.2009.03.001.

Roark, R.J., Young, W.C., & Plunkett, R. (1976). Formulas for stress and strain. ??

Roudsari, M.T., Jamshidi K.H., & Moradi, S.H. (2018). Experimental and numerical assessment of reduced IPE beam sections connections with box-stiffener. *International Journal of Steel Structures*, *18*(1), 255-263. https://doi.org/https://doi.org/10.1007/s13296-018-0319-0.

Sedaghatnezhad, H., Fallah, A., & Mosalman Yazdi, M. (2021). Probabilistic Seismic Demand Assessment of chevron bracing Steel Moment Frames with TADAS damper. *Journal of Seismology and Earthquake Engineering*, *23*(4). https://doi.org/10.48303/jsee.2023.1987344.1045

Shadman Heidari, P., Aziminejad, A., Moghadam, A.S., & Jafari, M.A. (2020). Evaluation of drilled

flange connections with combined arrangements of holes and notches. *Bulletin of Earthquake Engineering*, *18*(14), 6487-6532. https://doi.org/https://doi.org/10.1007/s10518-020-00920-1.

Tabar, A.M., Alonso-Rodriguez, A., & Tsavdaridis, K.D. (2022). Building retrofit with reduced web (RWS) and beam (RBS) section limited-ductility connections. *Journal of Constructional Steel Research*, *197*, 107459. https://doi.org/https://doi.org/10.1016/j.jcsr.2022.107459.

TahamouliRoudsari, M., Cheraghi, K., & Aghayari, R. (2022). Investigating the retrofit of RC frames using TADAS yielding dampers. *Structural Durability \& Health Monitoring*, 16(4), 343-359. https://doi.org/https://doi.org/10.32604/sdhm.2022.07927.

TahamouliRoudsari, M., Cheraghi, K., & Habibi, M. R. (2019). Investigation of retrofitting RC moment resisting frames with ADAS yielding dampers. *Asian Journal of Civil Engineering*, *20*(1), 125-133. https://doi.org/https://doi.org/10.1007/s42107-018-0092-6.

TahamouliRoudsari, M., Jamshidi K.H., Torkaman, M., & Ganji M.S. (2018). Experimental and numerical investigations of rigid IPE beam connections with drilled flange and web stiffener. *Structures*, *16*, 303-316. https://doi.org/https://doi.org/10.1016/j.istruc.2018.10.008.

Vajdian, M., Parvari, A., & Afzali, M. (2020). Improvement of seismic performance of beam-column connection with replaceable drilled attachment parts. *Periodica Polytechnica Civil Engineering*, *64*(4), 1202-1218. https://doi.org/https://doi.org/10.3311/PPci.15239.

Vajdian, M., Zahraei, S.M., Mirhosseini, S.M., & Zeighami, E. (2020). Investigation of seismic performance of (RBS) and Drilled Flange Connection (DFC) containing rhombus shaped hole in steel moment frames. *Australian Journal of Civil Engineering*, 18(2), 246-262. https://doi.org/https://doi.org/10.1080/14488353.2020.1771664.

Zahrai, S.M., & Heisami, A. (2017). Seismic performance of tall buildings with impact damper under near and far-field earthquakes. *Journal of Seismology and Earthquake Engineering*, *19*(4), 327-336. http://www.jsee.ir/article_240774_4ff751b54248cf14ba4fe7608fdb6cc0.pdf.

Nomenclature

D : The diameter of the flange hole
F_u: The critical axial load of the column
α: Hole-to-flange cross-section area ratio
t_s: The thickness of the SRD
L: The width of the SRD
R: The radius of SRD
σ_{y_s} : The yield stress of SRD
K_s: Elastic stiffness of SRD
E: Young's beam modulus
t_w: The thickness of the web beam
M_p: Plastic moment of the beam equipped with SRD
M_b: The contribution of the beam moment to the total moment
σ_{y_b} : The yield stress of the beam
d: The distance from the column to the middle of the weakened place of the beam